analytical chemistry

Article

pubs.acs.org/ac

# Dielectrophoresis-Assisted Raman Spectroscopy of Intravesicular Analytes on Metallic Pyramids

Avijit Barik,[†,‡] Sudhir Cherukulappurath,[†,§] Nathan J. Wittenberg,[†] Timothy W. Johnson,[†] and Sang-Hyun Oh*[,†,‡]

[†]Department of Electrical and Computer Engineering, [‡]Department of Biomedical Engineering, University of Minnesota, Minneapolis, Minnesota 55455, United States

Supporting Information

**ABSTRACT:** Chemical analysis of membrane-bound containers such as secretory vesicles, organelles, and exosomes can provide insights into subcellular biology. These containers are loaded with a range of important biomolecules, which further underscores the need for sensitive and selective analysis methods. Here we present a metallic pyramid array for intravesicular analysis by combining site-selective dielectrophoresis (DEP) and Raman spectroscopy. Sharp pyramidal tips act as a gradient force generator to trap nanoparticles or vesicles from the solution, and the tips are illuminated by a monochromatic light source for concurrent spectroscopic detection of trapped analytes. The parameters suitable for DEP trapping were optimized by fluorescence microscopy, and the Raman spectroscopy setup was characterized by a nanoparticle based model system. Finally, vesicles loaded with 4-mercaptopyridine were concentrated at the tips and their Raman spectra were detected in real time. These pyramidal tips can perform large-area array-based trapping and spectroscopic analysis, opening up possibilities to detect molecules inside cells or cell-derived vesicles.

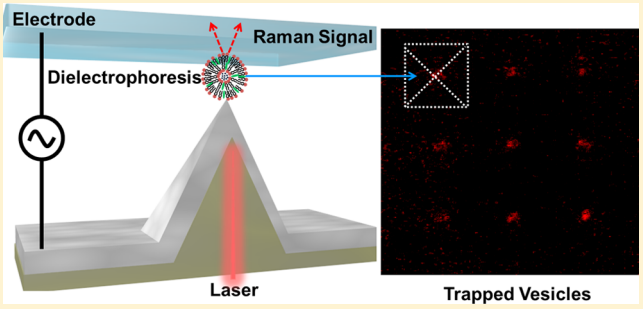




In cells many important molecules are packaged into small, membrane-bound containers. Examples include the nucleus, which contains DNA, organelles like mitochondria, lysosomes, endoplasmic reticuli, and Golgi apparatus, along with secretory vesicles that contain neurotransmitters, and extracellular membrane-bound particles like exosomes and platelet-derived microparticles. In addition to their contents, the lipid bilayer membranes that define the boundaries of these structures are embedded with proteins and decorated with carbohydrates. These subcellular structures can be labeled with specific fluorophores that allow positional tracking in space and time,[1] and there are a number of flourescent indicators that can detect concentration dynamics of chemical species.[2−6] These probes, however, are limited in that a unique probe must be used for each species of interest, and due to the breadth of fluorescence emission bands and band overlap, only a few different probes can be used simultaneously.

As an alternative to fluorescent methods and probes, vibrational spectroscopic techniques, such as Raman spectroscopy, offer the ability to chemically fingerprint the contents and membranes of liposomes[7] and organelles.[8] Raman peaks are chemically specific and much narrower than fluorescence emission bands, therefore a single spectrum can be used to identify many chemical species. Since the peaks in Raman spectra are intrinsic to the molecules being analyzed, no additional labels or tags are required. However, because Raman signals are inherently weak, it is often necessary to locally concentrate analyte molecules or place molecules in the vicinity of metallic films or nanostructures to harness the enhanced local optical fields, or a combination of both approaches.[9,10] This can be accomplished through the association of the analytes with metallic nanoparticles,[11,12] or the analytes can be selectively directed toward sharp features of metallic nanostructures that present a strong electromagnetic field confinement using DEP.[13−17]

Gradient forces generated by sharp metallic tips have been used to trap submicron particles that are polarizable with respect to the surrounding medium by DEP.[18,19] DEP forces originate from the difference in conductivity and permittivity between a polarizable particle and its surrounding medium. For a spherical particle of radius $R$, the time averaged DEP force is given by[20]

$$\vec{F}_{\mathrm{DEP}}(\omega) = \pi\varepsilon_{\mathrm{m}}R^3\cdot\mathrm{Re}(f_{\mathrm{CM}}(\omega))\nabla|E|^2 \quad (1)$$

where $\varepsilon_{\mathrm{m}}$ is the permittivity of the surrounding medium and $\mathrm{Re}(f_{\mathrm{CM}}(\omega))$ is the real part of the frequency $(\omega)$ dependent Clausius−Mossotti factor that determines the polarity of the force. On application of a bias, a metallic tip creates a large electric field gradient, $\nabla|E|^2$, due to the lightening-rod effect, and can attract and trap particles by positive DEP

**Received:** October 2, 2015
**Accepted:** December 25, 2015
**Published:** January 11, 2016

  

DOI: 10.1021/acs.analchem.5b03719
*Anal. Chem.* 2016, 88, 1704−1710

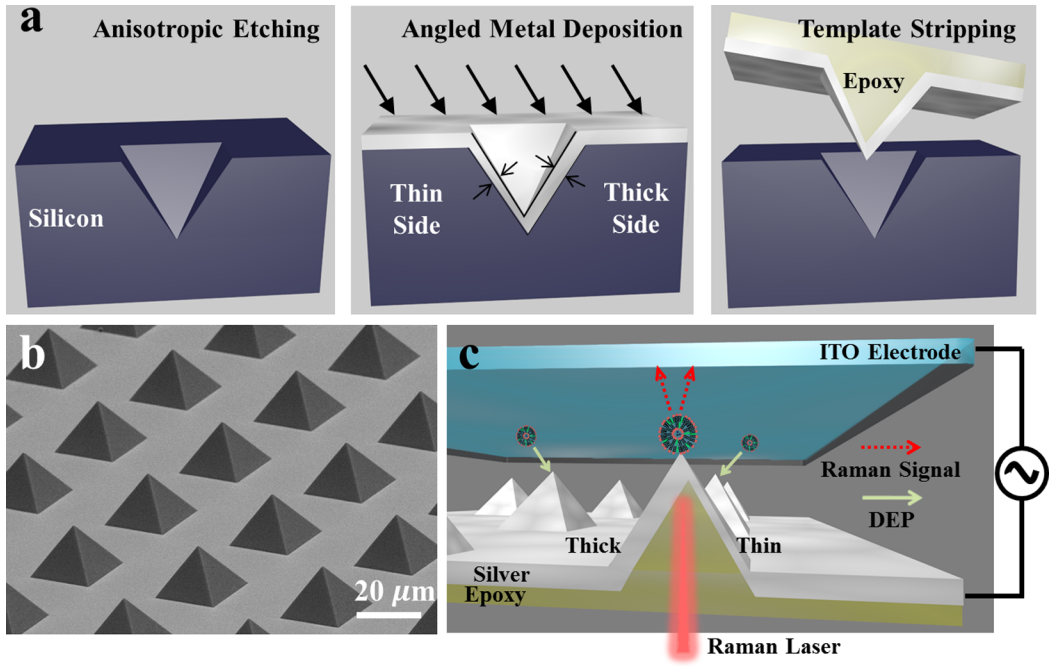


**Figure 1.** Fabrication of an asymmetric metallic pyramid array. (a) Schematic of the template-stripping method to fabricate an asymmetric pyramid array. First, pyramidal pits were made on silicon wafer by anisotropic KOH etching. Then, silver was evaporated at an angle of 10° from normal to impart asymmetry in the metal thickness on the two opposite faces of the pyramids. Finally, the asymmetric pyramid arrays were template-stripped and transferred onto a glass slide. (b) Scanning electron micrograph of template-stripped asymmetric pyramids with the base dimension of 20 $\mu$m × 20 $\mu$m. (c) Illustration of the experimental setup. A linearly polarized monochromatic light source is used to illuminate the asymmetric pyramid internally, and the far field scattered light from the tip of the pyramid is collected by a high NA objective. Particles are trapped on the tip of the pyramid by DEP, and their Raman scattering spectra are detected through the transparent indium tin oxide (ITO) electrode.

$(\mathrm{Re}(f_{\mathrm{CM}}(\omega)) > 0)$.[14] In the context of nano-optics, sharp metallic tips can also concentrate optical fields and act as a localized light source.[21]

In this work we made a large array of metallic pyramids, where a DEP-assisted concentration scheme is combined with optical illumination to rapidly detect Raman signals from trapped bioparticles. Conventional schemes for such tip-based probes, apart from being cumbersome, present practical limitations in integrating them in planar lab-on-a-chip type devices to detect analytes in a controlled fashion. In contrast, by integrating the optical excitation with the active concetration scheme on a planar array of pyramids, our setup is straightforward, simple, capable of multiplexing, and offers very low-background noise. Recently, we have demonstrated the application of metallic pyramidal tips with asymmetrically thick facets for enhanced Raman studies.[22] Here we use DEP for concentrating vesicles containing analyte molecules on an array of metallic pyramidal tips and simultaneously perform Raman spectroscopy to reveal the chemical nature of the intravesicular analyte molecules that are trapped at the tip.

## EXPERIMENTAL SECTION

**Fabrication of Asymmetric Metallic Pyramid Arrays.** Standard (100) silicon wafers were coated with a 100 nm-thick $Si_3N_4$ film by low-pressure chemical vapor deposition, followed by photolithography and reactive ion etching to pattern circular holes of 20 $\mu$m diameter. The wafers were then soaked in a bath containing 30% KOH, 10% isopropanol, and water to create sharp pyramidal pits through crystal-orientation-dependent anisotropic etching of silicon.[21] The nitride layer was then removed by soaking the wafers in a 49% HF acid bath for 30 min. Next, 135 nm silver was deposited at a tilted angle using electron-beam evaporator (CHA, SEC 600), producing an asymmetric thickness of metal layer on opposite facets of the pyramidal pit. Samples were placed at an angle of 10° with respect to the normal or (80° with respect to the sample holder), which resulted in a silver layer of thickness 40 nm on one pyramid face and 120 nm on the opposite face. Finally, the silver pyramid arrays were template-stripped and transferred to a glass slide by using UV-curable optical adhesive (Norland Products NOA 61, refractive index: 1.56) as a backing layer.[23] This fabrication method yielded about 100 000 pyramids on a 4-in. silicon wafer. A small area of the sample, which typically contains approximately a few thousand pyramidal tips, was used for the experiments.

**Preparation of Raman-Active Gold Nanoparticles.** A 50:50 mixture of 70 nm citrate-stabilized gold nanoparticles (AuNP, nanoComposix) and 5 mM 4-mercaptopyridine (4MP) solution was prepared and kept overnight to coat the nanoparticle surface with 4MP molecules. Next, the solution was centrifuged at 7500 r.p.m. for 30 min, then the supernatant was discarded. The nanoparticles were resuspended in water, and this process was repeated two more times.

**Preparation of Phospholipid Vesicles.** An 80:20 molar ratio mixture of 1,2-dimyristoyl-*sn*-glycero-3-phosphocholine (DMPC) and cholesterol in chloroform was dried overnight in a vacuum desiccator to remove all traces of chloroform. Next, the dried lipid mixture was rehydrated with water for at least 5 h at 50 °C to promote formation of a vesicle suspension. For experiments involving fluorescence microscopy, the vesicles were composed of a lipid mixture with 64 mol % DMPC, 16 mol % cholesterol, and 20 mol % 1,2-dimyristoyl-*sn*-glycero-3-phosphoethanolamine-*N*-lissamine Rhodamine B-sulfonyl, ammonium salt (Rhodamine-DMPE). The vesicles were extruded


DOI: 10.1021/acs.analchem.5b03719
*Anal. Chem.* 2016, 88, 1704−1710

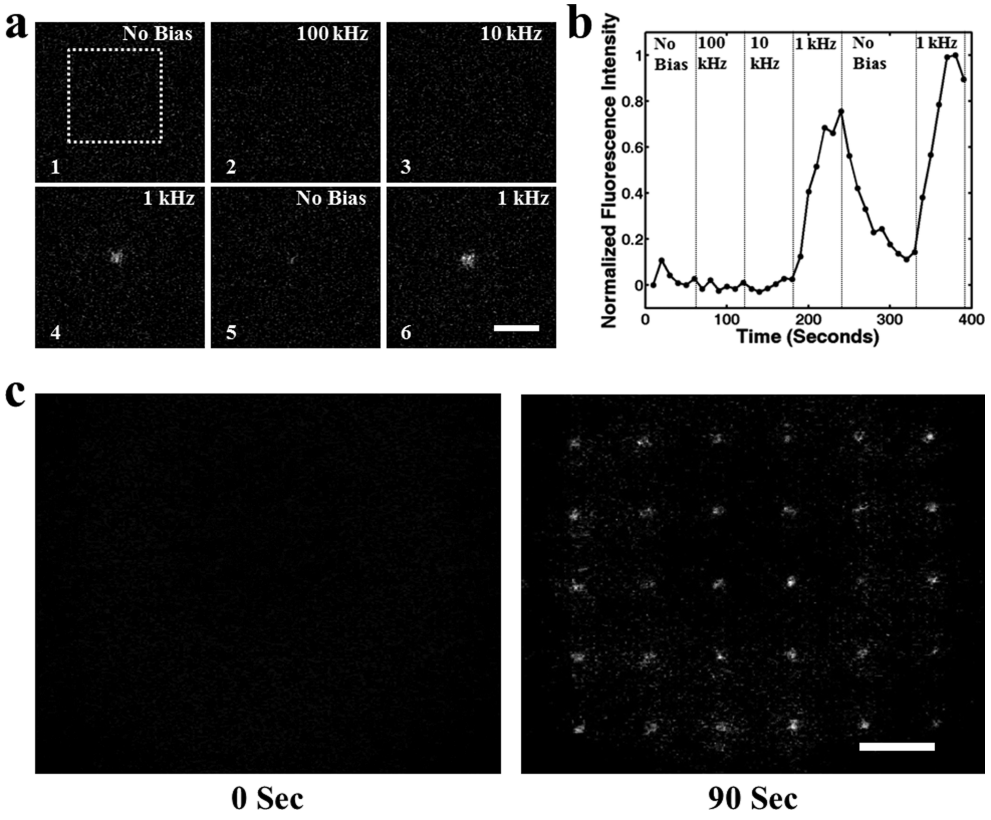


**Figure 2.** Frequency-dependent trapping of 200 nm diameter fluorescent vesicles across a pyramid array. (a) DEP trapping of vesicles depends on the applied frequency. The frequency was switched from 100 to 10 to 1 kHz in 60 s intervals with an applied bias of 10 Vpp. Trapping was first observed at 1 kHz, which also seems to be a reversible event as the vesicles diffused away from the tip on turning off the bias. An outline of the base of the pyramid (white line) is shown in the first frame. The scale bar is 10 $\mu$m. (b) Plot of the normalized fluorescence intensity from a 4 $\mu$m circle around the tip of a pyramid as a function of frequency for an applied bias of 10 Vpp. (c) A 5 × 6 pyramid array imaged to demonstrate the trapping capabilities across a pyramid array at 1 kHz frequency and 10 Vpp bias. The scale bar is 40 $\mu$m.

through a polycarbonate membrane with 200 nm pores (Avanti mini-extruder) to achieve uniform size distribution. All lipids were obtained as chloroform solutions from Avanti Polar Lipids.

For Raman spectroscopy, vesicles containing 4MP molecules were prepared. First, an 80:20 molar ratio mixture of DMPC and cholesterol was dried overnight in a vacuum desiccator to remove all traces of the chloroform suspending medium. Next, the dried lipid mixture was suspended in a 5 mM aqueous 4MP solution to form vesicles with 4MP molecules both inside and outside. The hydration step was performed overnight at 50 °C, which is above the miscibility phase transition temperature of the DMPC/cholesterol membrane.[24] Next, the vesicle solution was subjected to five freeze−thaw cycles to decrease the lamellarity of the vesicles and increase the 4MP encapsulation efficiency.[25] The solution was frozen in a mixture of dry ice and acetone (−78 °C) followed by thawing in a water bath at 50 °C to prepare vesicles with low lamellarity and higher 4MP content. After the freeze−thaw treatment, the vesicles were extruded through a polycarbonate membrane with 200 nm pores. Finally, the 4MP molecules outside the vesicles were removed from the solution by performing dialysis (Slide-A-Lyzer MINI Dialysis, Thermo Scientific) against a 1 L water bath with three water changes.

**DEP Trapping.** A sinusoidal alternating current (AC) bias with a peak-to-peak value varying between 8 to 10 V and a frequency of 1 kHz was applied between the top ITO coated glass slide (Sigma-Aldrich) and the bottom metallic pyramid electrode to create a DEP trap at the tip of each pyramid. The distance between the electrodes was defined by two layers of 3M Scotch magic tape, whose total thickness was measured to be approximately 80 $\mu$m (each layer is approximately 40 $\mu$m thick). All the solutions used is this work were prepapred in DI water and the final conductivity was approximately 2 $\mu$S/cm (measured by B-771 LAQUAtwin, Horiba Scientific).

**Fluorescence Microscopy.** A 50× objective (NA 0.55) was used to observe DEP trapping of 200 nm vesicles. A 532 nm laser was used to excite fluoroscence and the emitted light was collected using the same objective and passed through the appropriate filter. Fluorescence images were collected at regular intervals using a Thorlabs CCD camera.

**Raman Spectroscopy.** A 785 nm laser was used to illuminate a single asymmetric pyramid in an internal illumination mode through a 20× objective (NA 0.45) at normal incidence. Far-field scattered light from the tip of the pyramid was collected through the transparent top electrode by a 50× objective (NA 0.55). The collected light was passed through a 785 nm notch filter, then sent to a fiber-coupled spectrometer (Ocean Optics QE65000). Raman spectra were collected and analyzed using Spectra Suite software.

## RESULTS AND DISCUSSION

A schematic of the fabrication procedure is illustrated in Figure 1a. A combination of photolithography, anisotropic etching, angled metal evaporation, and template stripping (transfer of metal layer onto a glass slide by using an adhesive) was used to


DOI: 10.1021/acs.analchem.5b03719
*Anal. Chem.* 2016, 88, 1704−1710

fabricate an array of asymmetric pyramids, as described in our previous work.[22] A scanning electron micrograph (SEM) of the pyramid array (Figure 1b) shows the base dimension of each pyramid to be 20 $\mu$m × 20 $\mu$m, and the periodicity of the array is 40 $\mu$m. The experimental setup for performing DEP and Raman/fluorescence detection is systematically shown in Figure 1c. After injecting 5 $\mu$L of the vesicle solution, an ITO-coated glass slide was placed on top. The tip of the pyramid was approximately 66 $\mu$m away from the ITO electrode (height of each pyramid is ∼14 $\mu$m). An AC voltage was applied to generate a strong electric field gradient at the tip of the pyramid to act as a DEP trap.[14] For fluorescence microscopy a 532 nm laser was used in epifluorescence mode (illumination and collection through the top ITO slide) using a 50× objective (not shown in the schematic). For Raman spectroscopy, a 785 nm diode laser was loosely focused at the tip of a single pyramid from the backside using a 20× objective (NA 0.45). The pyramids were designed to form a plasmonic hot spot around their tip while not needing to illuminate other parts of the structure. This is made possible by the angled-deposition, which deposits different thickness of silver on opposing facets of the pyramid. When illuminated internally, free-space light is coupled from the backside through a Kretschmann-like method across the thin facet of the pyramid, and into plasmons on the top-side of the pyramid. By this way it is possible to create plasmons on the top-side around the tips while most of the incident light is reflected by the optically thick silver everywhere else. The plasmons on the top-side then travel up the face of the pyramid and are partially scattered into free-space light when they reach the tip. The far-field scattered light from the tip was collected using a 50× objective. The power of the laser was approximately 5 mW, which is not high enough in this setup to induce trapping due to optical gradient forces or induce significant thermal effects. A detailed investigation of the internal illumination scheme was performed in our previous work.[22] This scheme of Raman spectroscopy offers certain advantages over confocal methods. First, unlike the confocal method, we collect the Raman signal from a highly localized point (single illuminated pyramid tip). This results in a spatial resolution that is limited to the area of the tip. Second, the readout of the spectrum is faster in this method as the illuminated region is very small. Finally, the set up used in this scheme is simpler, compact, and provides real-time in situ measurement capabilities.

Fluorescence microscopy was used to observe DEP trapping of small unilamellar vesicles (SUVs) in real time. In the presence of an electric field, charge separation occurs at the interface of the lipid membrane and the surrounding medium, enabling DEP trapping toward the pyramidal tip.[26,27] The results of trapping 200 nm fluorescent vesicles are shown in Figure 2. The frequency of the AC signal was varied from 100 to 1 kHz at 1 min intervals, where the voltage was kept constant at 10 Vpp (peak-to-peak voltage). The trapping was first observed at a frequency of 1 kHz (Figure 2a), which also seems to be a reversible event—the vesicles moved away from the tip once the signal was switched off, and they were trapped again as the voltage was turned back on. It does not appear the vesicles rupture upon encountering the bare metal surface, which is in line with previous findings.[28] Furthermore, we monitored the normalized fluorescence intensity at the tip of a pyramid (region of interest is a circle of diameter 4 $\mu$m) as the frequency was varied (Figure 2b). The intensity plot demonstrates the same pattern of events as described in Figure 2a. The fluorescence signal increases as vesicles are transported to the tip of the pyramid by DEP. However, the transport of vesicles from the bulk solution is diffusion limited. As soon as we turn off the bias the vesicles are released from the trap but they stay close to the tip—resulting in a nonzero signal around 320 s. In the next cycle of DEP, as the number of vesicles near the tip is already higher, it is possible to trap an even larger number of vesicles—causing greater fluorescence peak intensity around 390 s. Figure 2c shows the ability to capture the vesicles on a large-scale pyramid array. A 5 × 6 pyramid array was imaged before and after DEP trapping with 1 kHz frequency and 10 Vpp bias, which shows the vesicles were captured at the tips across the array.

To demonstrate the label-free detection capability of our platform by Raman spectroscopy, we chose gold nanoparticles coated with 4MP molecules (AuNP-4MP) as target particles. Owing to the large difference in conductivity between the metallic nanoparticles and the suspending water medium, it is straightforward to trap them on the pyramid tips using DEP. Also 4MP molecules are well-known for their large scattering cross sections and they can readily form a self-assembled monolayer on the metal surface by thiol−metal covalent bonding.[29] AuNP-4MP particles were trapped at the tip of the pyramid by applying a voltage of 8 Vpp at a frequency of 1 kHz and the Raman signal was collected simultaneously. As the gold nanoparticles are trapped by DEP, the 4MP molecules attached to its outer surface are brought close to the pyramid tip, which enhances the scattered Raman signal. Previously we demonstrated plasmonic nanofocusing using asymmetrically thick template-stripped metallic pyramids. We showed an enhancement of Raman scattering signals by an order of $10^4$ when the pyramid is internally illuminated.[22] Figure 3a depicts the Raman spectra collected during DEP with 2 s acquisition time, which shows the appearances of signature Raman peaks from 4MP molecules.[30] The peaks at 1013, 1065, 1099, and 1584 $cm^{-1}$ are assigned to the ring-breathing mode, the in-plane C−H bend, the ring-breathing mode coupled with the $\nu$(C−S) stretching mode, and the ring-stretching mode, respectively.[31−33] The same experiment was repeated with bare AuNP as a negative control experiment, which does not show the characteristic Raman peaks from 4MP (Figure 3b). The broad peak centered around 1400 $cm^{-1}$ can be attributed to autofluorescence from the glass substrate at this excitation wavelength. To confirm that the AuNP-4MP particles are trapped primarily at the tip and that the enhanced Raman signals are indeed coming from the tip of the pyramid, we positioned the laser spot at different regions of the pyramid and collected Raman signal with 10 s acquisition time. The result of this experiment is shown in Figure 3c. The signal is very weak when the laser spot is focused on the facets but the signal enhances significantly upon focusing at the tip of the pyramid. Using higher acquisition time as compared to Figure 3a improves the signal quality, as evident from the appearance of another Raman peak around 1226 $cm^{-1}$ that is assigned to the in-plane C−H bend.[32] We believe that the signal is contributed to by the DEP trapping and clustering of nanoparticles,[17,34] as well as the plasmonic nanofocusing effect. Furthermore, we also demonstrate the reproducibility of this technique across multiple pyramids as shown in Figure 3d.

Next, our platform was used to detect the contents of vesicles through DEP-assisted Raman spectroscopy. The vesicle suspension was prepared by hydrating an 80:20 molar ratio mixture of DMPC and cholesterol with a 5 mM aqueous 4MP


DOI: 10.1021/acs.analchem.5b03719
Anal. Chem. 2016, 88, 1704−1710

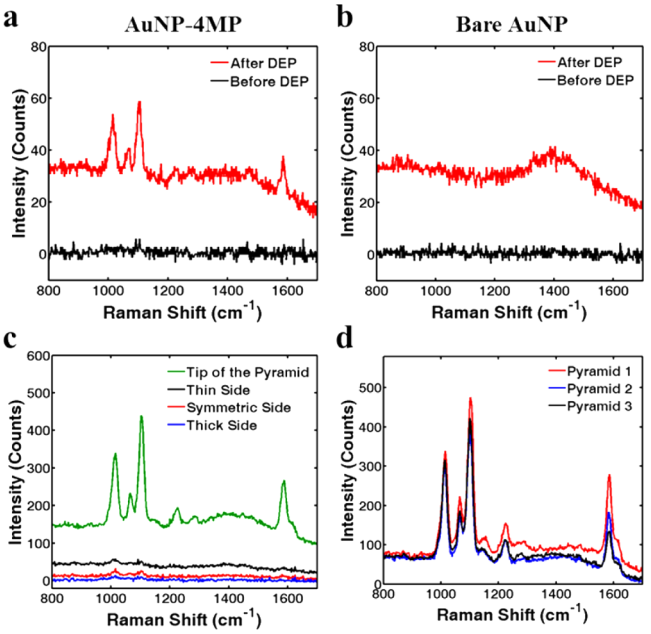


**Figure 3.** DEP-assisted Raman spectroscopy of AuNP-4MP. (a) Raman signal collected before and after DEP trapping of AuNP-4MP on the tip of the pyramid. (b) Negative control experiment with bare AuNP showing disappearance of characteristic Raman peaks from 4MP. The acquisition time used in parts a and b was 2 s. (c) Raman scattering spectra obtained when illuminating at different regions of the pyramid. The red spectrum was obtained when the illumination is on the symmetric facets while the blue and black spectra were obtained when the laser spot was on the thick and thin facets, respectively. The green spectrum is obtained when the laser spot was on the apex. Clearly, the signal is strongest when the laser was focused at the tip. (d) Raman signal collected across multiple pyramids to demonstrate the repeatability and parallel trapping capability of this technique. A 10 s acquisition time was used for parts c and d.

solution. 4MP molecules were captured within the vesicles during the hydration process, which is facilitated by the presence of cholesterol molecules that help in tighter packing of lipid molecules to reduce leakage.[35] An illustration of a vesicle containing 4MP molecules is shown in Figure 4a. After three rounds of dialysis, the concentration of 4MP molecules outside the vesicles was reduced significantly to approximately 12 fM (calculation in the Supporting Information) while the concentration inside was 5 mM. For trapping, an 8 Vpp potential was applied at a frequency of 1 kHz, and the Raman signal (2 s acquisition time) was collected from a single pyramid tip by using a 785 nm diode laser at 2 s intervals. Figure 4b shows the real-time Raman signal, which clearly demonstrates the detection of 4MP molecules over time. The signals are offset by 20 counts from each other for better representation. Within 60 s of DEP, we observed a signal-to-noise ratio (S/N) of 208 and 326 at the Raman peak 1013 and 1099 $cm^{-1}$ respectively. As our experimental setup offers low background and high S/N in a fast manner, we believe it can also be used for experiments demanding low detection limits.[36] Furthermore, control experiments confirmed that we are indeed detecting 4MP molecules from inside the vesicles (Figure 4c). For each measurement the AC bias (8 Vpp and 1 kHz frequency) was on for 60 s and the Raman signal was compared with an acquisition time of 2 s. The first control experiment was done with a vesicle-free, 12 fM 4MP solution, which is the same concentration as in the suspending medium of the vesicles after dialysis. No Raman signal was observed as represented by the red curve in Figure 4c.

Next we estimated the concentration of 4MP molecules in solution in the event of complete lysis of all vesicles containing 5 mM 4MP, assuming the total vesicular 4MP content would be homogeneously redistributed into the suspending medium. Each vesicle was modeled as a 200 nm diameter unilamellar sphere and the total number of vesicles was calculated by estimating the number of lipid molecules per vesicle. Complete lysis of all vesicles containing 5 mM 4MP would result in a solution of 24 $\mu$M 4MP concentration. Details of the calculation can be found in the Supporting Information. Therefore, we collected Raman signals from pyramids in the presence of 24 $\mu$M 4MP. The Raman signal (black curve in Figure 4c) was significantly smaller than the signal obtained from the 4MP molecules inside the vesicles. The difference in the intensity is due to the confinement of 4MP molecules within the vesicles and this setup enables us to detect intravesicular content without rupturing the vesicles. The blue curve corresponds to the baseline, which is consistent across different experiments and is a characteristic of the optical setup. We believe the overall increase in scattered background in case of vesicle trapping (green curve) may be due to the lensing effect induced by the incident light, which is not completely filtered by the notch filters.

To investigate the source of observed Raman signals, the normalized Raman intensity at 1013 $cm^{-1}$ was monitored over time. As evident from Figure 4d, we do not obtain any Raman signal from the floating vesicles containing 5 mM 4MP before turning on the bias. The signal starts to rise once we turn on DEP trapping of vesicles at the tip of the pyramid, but it does not disappear on turning off the bias. One explanation is leakage of 4MP molecules in the presence of large electric field at the pyramid tip. It is possible to create pores in the vesicle membrane by applying oscillating electric field, which generates large transmembrane potential across the membrane and breaks down the phospholipid bilayer.[37,38] However, as we move further from the tip, the strength of the electric field decays (supplementary Figure S1b) and the likelihood of vesicle leakage is less. Hence, locally concentrated vesicles can release 4MP molecules at the tip, where it can stick due to thiol−metal covalent bonding.[29] Another possibility is that some of the 4MP could leak from the vesicles upon DEP-induced adsorption to the pyramid tips. This would be due to membrane defects caused by the increase in the vesicle membrane tension that accompanies adsorption.[39] However, previous results have shown that for isolated small (<100 nm-diameter) vesicles adsorbed on quartz substrates there is little leakage of encapsulated small molecules until the vesicles rupture to form planar membranes.[40] Vesicles generally do no rupture on bare metal surfaces such as silver, and vesicle adhesion to them is much weaker than to hydrophilic surfaces like quartz, glass, or $SiO_2$, upon which vesicles rupture.[41] The weaker adhesion of vesicles on silver would attenuate any increase in membrane tension upon adsorption. This is also evident from the decay in fluorescent signal in Figure 2b, which suggests that the vesicles do not stick to the pyramid tip and diffuse away on turning off the bias. Hence, the presence of Raman signal after the vesicles are removed can be explained by an electric-field-induced leakage mechanism as explained above. Furthermore, the presence of cholesterol molecules in the membrane also enables tighter packing among lipid molecules, thus reducing the likelihood of any unwanted 4MP leakage in


DOI: 10.1021/acs.analchem.5b03719
Anal. Chem. 2016, 88, 1704−1710

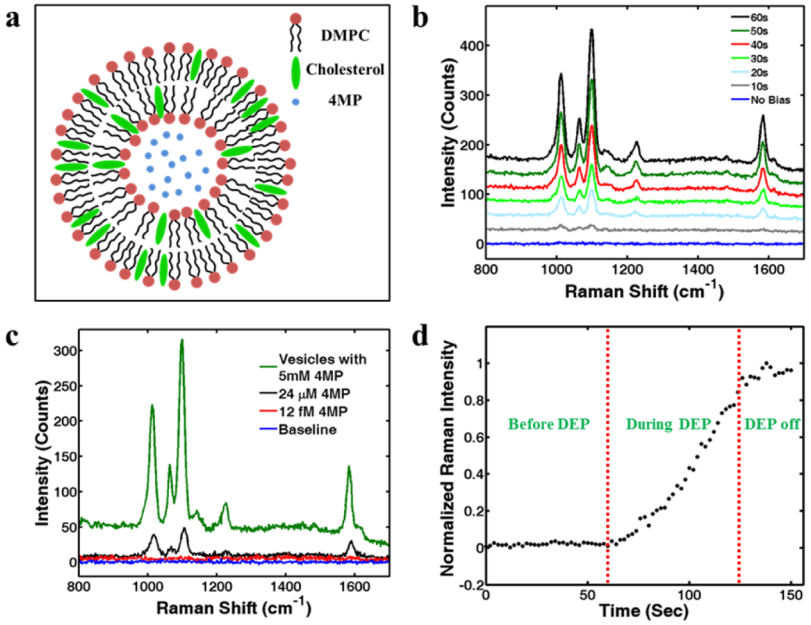


**Figure 4.** Detecting molecules encapsulated in vesicles with DEP-assisted Raman spectroscopy. (a) Illustration of a DMPC/cholesterol vesicle encapsulating 4MP molecules. The surrounding medium is water. (b) Real-time Raman signal collected from the tip of the pyramid while trapping the vesicles using DEP. The signals are offset by 20 counts for clarity. The acquisition time for each measurement was 2 s. (c) Comparison of the signal obtained from the 4MP molecules inside the trapped vesicles on the tip of the pyramid (green curve) to control experiments representing the concentration of free, unencapsulated 4MP after dialysis (12 fM, red curve), and the 4MP concentration in the event of complete vesicle lysis (24 $\mu$M, black curve). The blue curve corresponds to the baseline, which is consistent across different experiments and is a characteristic of the optical setup. The acquisition time for each measurement was 2 s. (d) The normalized intensity of the Raman peak at 1013 $cm^{-1}$ is plotted as a function of time to demonstrate the evolution of Raman signal from 4MP as we perform DEP trapping of vesicles.

the solution. This ensures a steady 4MP concentration outside the vesicles and leakage may only happen in the presence of strong electric field at the tip of the pyramid.

## CONCLUSION

Here, we have built a platform to detect analyte molecules loaded within small vesicles in a label-free manner by combining Raman spectroscopy and DEP. This setup can be useful in lab-on-a-chip type devices used to study subcellular structures that are extracted from cellular environments using various pretreatment procedures.[42,43] We have utilized a large array of metallic pyramids for DEP-assisted Raman spectroscopy of analytes either encapsulated in nanoscopic containers or attached to nanoparticles. Metallic pyramid tips harnessing strong electric field gradient was used to facilitate fast and directed transport by DEP, which was used to trap 200 nm vesicles and 70 nm gold nanoparticles. The efficiency of DEP trapping can be further improved by reducing the distance between the electrodes, which enables application of lower voltages or usage of lower concentration of particles. When illuminated internally with linearly polarized light, the asymmetry in metal thickness on the opposite facets of the pyramid can focus light into subwavelength hotspots at the tip. We coupled this nanofocusing capability of the pyramidal tips with DEP preconcentration to extract spectral information on analytes in a fast manner. To demonstrate this scheme, Raman scattering signals were obtained from 4MP molecules adhered to AuNP. In order to test the scheme on biologically relevant model systems, vesicles containing 4MP molecules were trapped at the tip using DEP and Raman signals from the intravesicular 4MP were detected in real time. This technique will open up several possibilities in developing optofluidic nanosensors that are capable of fingerprinting the molecules in cellular environments. For example, secretory vesicles store neurotransmitters at concentrations ranging from 100 mM to nearly 1 M.[44−47] Using our method isolated vesicles containing neurotransmitters could be rapidly concentrated at pyramid tips and chemically identified via their Raman spectra. Additionally, this method could be used to spectroscopically identify and quantify encapsulated drugs in nanoparticle or liposomal drug delivery preparations, potentially down to the single nanoparticle or single liposome level.

## ASSOCIATED CONTENT

### Supporting Information

The Supporting Information is available free of charge on the ACS Publications website at DOI: 10.1021/acs.analchem.5b03719.

Additional information as noted in text (PDF)

## AUTHOR INFORMATION

### Corresponding Author

*E-mail: sang@umn.edu.

### Present Address

§(S.C.) Department of Physics, Goa University, Taleigao Plateau, Goa, 403206, India.

### Notes

The authors declare no competing financial interest.

## ACKNOWLEDGMENTS

This work was supported by the National Science Foundation (NSF CAREER Award and CMMI 1363334), the National Institutes of Health (R01GM092993), and the MnDrive



DOI: 10.1021/acs.analchem.5b03719
*Anal. Chem.* 2016, 88, 1704−1710

Initiative from the State of Minnesota. A.B. acknowledges support from the University of Minnesota Doctoral Dissertation Fellowship. Device fabrication was performed at the Minnesota Nanofabrication Center, which receives support from the NSF through the National Nanotechnology Coordinated Infrastructure (NNCI). Parts of this work were carried out in the Characterization Facility, University of Minnesota, which receives partial support from NSF through the MRSEC program. Computational modeling was carried out using software provided by the University of Minnesota Supercomputing Institute.

## REFERENCES

(1) Shim, S.-H.; Xia, C.; Zhong, G.; Babcock, H. P.; Vaughan, J. C.; Huang, B.; Wang, X.; Xu, C.; Bi, G.-Q.; Zhuang, X. *Proc. Natl. Acad. Sci. U. S. A.* **2012**, *109*, 13978−13983.
(2) Grynkiewicz, G.; Poenie, M.; Tsien, R. Y. *J. Biol. Chem.* **1985**, *260*, 3440−3450.
(3) Belousov, V. V.; Fradkov, A. F.; Lukyanov, K. A.; Staroverov, D. B.; Shakhbazov, K. S.; Terskikh, A. V.; Lukyanov, S. *Nat. Methods* **2006**, *3*, 281−286.
(4) Galietta, L. J.; Haggie, P. M.; Verkman, A. *FEBS Lett.* **2001**, *499*, 220−224.
(5) Gee, K. R.; Zhou, Z.-L.; Qian, W.-J.; Kennedy, R. *J. Am. Chem. Soc.* **2002**, *124*, 776−778.
(6) Imamura, H.; Nhat, K. P. H.; Togawa, H.; Saito, K.; Iino, R.; Kato-Yamada, Y.; Nagai, T.; Noji, H. *Proc. Natl. Acad. Sci. U. S. A.* **2009**, *106*, 15651−15656.
(7) Schaefer, J. J.; Ma, C.; Harris, J. M. *Anal. Chem.* **2012**, *84*, 9505−9512.
(8) Klein, K.; Gigler, A. M.; Aschenbrenner, T.; Monetti, R.; Bunk, W.; Jamitzky, F.; Morfill, G.; Stark, R. W.; Schlegel, J. *Biophys. J.* **2012**, *102*, 360−368.
(9) Bantz, K. C.; Meyer, A. F.; Wittenberg, N. J.; Im, H.; Kurtulus, O.; Lee, S. H.; Lindquist, N. C.; Oh, S.-H.; Haynes, C. L. *Phys. Chem. Chem. Phys.* **2011**, *13*, 11551−11567.
(10) Stöckle, R. M.; Suh, Y. D.; Deckert, V.; Zenobi, R. *Chem. Phys. Lett.* **2000**, *318*, 131−136.
(11) Nie, S. M.; Emery, S. R. *Science* **1997**, *275*, 1102−1106.
(12) Dasary, S. S. R.; Singh, A. K.; Senapati, D.; Yu, H.; Ray, P. C. *J. Am. Chem. Soc.* **2009**, *131*, 13806−13812.
(13) Barik, A.; Otto, L. M.; Yoo, D.; Jose, J.; Johnson, T. W.; Oh, S.-H. *Nano Lett.* **2014**, *14*, 2006−2012.
(14) Jose, J.; Kress, S.; Barik, A.; Otto, L. M.; Shaver, J.; Johnson, T. W.; Lapin, Z. J.; Bharadwaj, P.; Novotny, L.; Oh, S.-H. *ACS Photonics* **2014**, *1*, 464−470.
(15) Chrimes, A. F.; Khoshmanesh, K.; Stoddart, P. R.; Kayani, A. A.; Mitchell, A.; Daima, H.; Bansal, V.; Kalantar-zadeh, K. *Anal. Chem.* **2012**, *84*, 4029−4035.
(16) Chrimes, A. F.; Kayani, A. A.; Khoshmanesh, K.; Stoddart, P. R.; Mulvaney, P.; Mitchell, A.; Kalantar-zadeh, K. *Lab Chip* **2011**, *11*, 921−928.
(17) Cherukulappurath, S.; Lee, S. H.; Campos, A.; Haynes, C. L.; Oh, S.-H. *Chem. Mater.* **2014**, *26*, 2445−2452.
(18) Tuukkanen, S.; Toppari, J. J.; Kuzyk, A.; Hirviniemi, L.; Hytönen, V. P.; Ihalainen, T.; Törmä, P. *Nano Lett.* **2006**, *6*, 1339−1343.
(19) Hunt, T.; Westervelt, R. *Biomed. Microdevices* **2006**, *8*, 227−230.
(20) Pohl, H. A. *Dielectrophoresis*; Cambridge University Press: Cambridge, England, 1978.
(21) Lindquist, N. C.; Nagpal, P.; McPeak, K.; Norris, D. J.; Oh, S.-H. *Rep. Prog. Phys.* **2012**, *75*, 036501.
(22) Cherukulappurath, S.; Johnson, T. W.; Lindquist, N. C.; Oh, S.-H. *Nano Lett.* **2013**, *13*, 5635−5641.
(23) Nagpal, P.; Lindquist, N. C.; Oh, S.-H.; Norris, D. J. *Science* **2009**, *325*, 594−597.
(24) Almeida, P. F.; Vaz, W. L.; Thompson, T. *Biochemistry* **1992**, *31*, 6739−6747.
(25) Mayer, L. D.; Hope, M. J.; Cullis, P. R.; Janoff, A. S. *Biochim. Biophys. Acta, Biomembr.* **1985**, *817*, 193−196.
(26) Dimova, R.; Bezlyepkina, N.; Jordö, M. D.; Knorr, R. L.; Riske, K. A.; Staykova, M.; Vlahovska, P. M.; Yamamoto, T.; Yang, P.; Lipowsky, R. *Soft Matter* **2009**, *5*, 3201−3212.
(27) Desai, S. P.; Vahey, M. D.; Voldman, J. *Langmuir* **2009**, *25*, 3867−3875.
(28) Reimhult, E.; Hook, F.; Kasemo, B. *Langmuir* **2003**, *19*, 1681−1691.
(29) Kumar, S.; Cherukulappurath, S.; Johnson, T. W.; Oh, S.-H. *Chem. Mater.* **2014**, *26*, 6523−6530.
(30) Bryant, M. A.; Joa, S. L.; Pemberton, J. E. *Langmuir* **1992**, *8*, 753−756.
(31) Wang, Y.; Sun, Z.; Hu, H.; Jing, S.; Zhao, B.; Xu, W.; Zhao, C.; Lombardi, J. R. *J. Raman Spectrosc.* **2007**, *38*, 34−38.
(32) Wang, Z.; Rothberg, L. J. *J. Phys. Chem. B* **2005**, *109*, 3387−3391.
(33) Baldwin, J.; Schühler, N.; Butler, I. S.; Andrews, M. P. *Langmuir* **1996**, *12*, 6389−6398.
(34) Romo-Herrera, J. M.; Alvarez-Puebla, R. A.; Liz-Marzán, L. M. *Nanoscale* **2011**, *3*, 1304−1315.
(35) Papahadjopoulos, D.; Nir, S.; Ohki, S. *Biochim. Biophys. Acta, Biomembr.* **1972**, *266*, 561−583.
(36) Hardcastle, C. D.; Harris, J. M. *Anal. Chem.* **2015**, *87*, 7979−7986.
(37) Neumann, E.; Sowers, A.; Jordan, C. *Electroporation and Electrofusion in Cell Biology*; Plenum: New York, 1989.
(38) Tsong, T. Y. *Biophys. J.* **1991**, *60*, 297−306.
(39) Seifert, U. *Adv. Phys.* **1997**, *46*, 13−137.
(40) Johnson, J. M.; Ha, T.; Chu, S.; Boxer, S. G. *Biophys. J.* **2002**, *83*, 3371−3379.
(41) Keller, C. A.; Kasemo, B. *Biophys. J.* **1998**, *75*, 1397−1402.
(42) Gao, J.; Yin, X.-F.; Fang, Z.-L. *Lab Chip* **2004**, *4*, 47−52.
(43) Kim, J.; Johnson, M.; Hill, P.; Gale, B. K. *Integr. Biol.* **2009**, *1*, 574−586.
(44) Finnegan, J. M.; Pihel, K.; Cahill, P. S.; Huang, L.; Zerby, S. E.; Ewing, A. G.; Kennedy, R. T.; Wightman, R. M. *J. Neurochem.* **1996**, *66*, 1914−1923.
(45) Colliver, T. L.; Pyott, S. J.; Achalabun, M.; Ewing, A. G. *J. Neurosci.* **2000**, *20*, 5276−5282.
(46) Omiatek, D. M.; Dong, Y.; Heien, M. L.; Ewing, A. G. *ACS Chem. Neurosci.* **2010**, *1*, 234−245.
(47) Omiatek, D. M.; Bressler, A. J.; Cans, A.-S.; Andrews, A. M.; Heien, M. L.; Ewing, A. G. *Sci. Rep.* **2013**, *3*, 1447.


DOI: 10.1021/acs.analchem.5b03719
*Anal. Chem.* 2016, 88, 1704−1710